Exploring the conformational landscape, hydrogen bonding and internal dynamics in the diallyl ether and diallyl sulfide monohydrates

Weslley G. D. P. Silva[1,2,a], Tamanna Poonia[1,a], Jennifer van Wijngaarden[1,3]*

[1]Department of Chemistry, University of Manitoba, Winnipeg, Manitoba, R3T 2N2, Canada

[2]I. Physikalisches Institut, Universität zu Köln, Zülpicher Str. 77, 50937 Köln, Germany

[3]Department of Chemistry, York University, Toronto, Ontario M3J 1P3, Canada

[a]Authors contributed equally
*Corresponding author

Email: vanwijng@yorku.ca
Phone: (437)460-3119

Abstract

The conformational spaces of the diallyl ether (DAE) and diallyl sulfide (DAS) monohydrates were explored using rotational spectroscopy from 6-19 GHz. Calculations at the B3LYP-D3(BJ)/aug-cc-pVTZ level suggested significant differences in their conformational behaviour, with DAE-w exhibiting 22 unique conformers and DAS-w featuring three stable structures within 6 kJ mol^{-1}, however, only transitions from the lowest energy conformer of each were experimentally observed. Spectral analysis confirmed that binding with water does not alter the conformational preference for the lowest energy structure of the monomers but it does influence the relative stabilities of all other conformers, particularly in the case of DAE. Non-covalent interaction (NCI) and quantum theory of atoms in molecules (QTAIM) analyses showed that the observed conformer for each complex is stabilized by two intermolecular hydrogen bonds (HBs), where water primarily interacts with the central oxygen or sulfur atom of the diallyl compounds, along with secondary interactions involving the allyl groups. The nature of these interactions was further elucidated using symmetry-adapted perturbation theory (SAPT) which suggests that the primary HB interaction with S in DAS is weaker and more dispersive in nature compared to the primary HB in DAE. This supports the experimental observation of a tunneling splitting exclusively in the rotational spectrum of DAS-w as the weaker contact allows water to undergo internal motions within the complex as shown based on calculated transition state structures for possible tunneling pathways.

*Introduct*ion

The omnipresence of water in nature and its ability to influence the structure and reactivity of molecules in chemistry and biology has long been of great interest to researchers.[1–5] The ability of water to stabilize the different geometries of highly flexible molecules through formation of intermolecular contacts is central to understanding solvation processes at the molecular level and can be probed experimentally using high resolution spectroscopic techniques. This is particularly true within the Fourier transform microwave spectroscopy community, given the power of this technique to precisely differentiate the unique conformations of molecules and their complexes with partner molecules (e.g., water) in a step-wise fashion in a cold molecular beam.[6–10] From a fundamental perspective, investigating microsolvated complexes as prototypes of solvation allows us to explore the correlation between the nature of non-covalent interactions and molecular dynamics (e.g., quantum tunneling, large amplitude motions) on the microscopic scale.[11–17] Hydrogen bonding (HB) emerges as the most dominant and indispensable non-covalent interaction responsible for stabilizing molecules and their complexes.[18–26]

HBs involving oxygen and sulfur have garnered considerable interest due to their influence on the structure and function of proteins, including protein hydration, self-assembly, and overall folding.[27–30] Despite their importance, however, sulfur HBs are still not well-characterized at the molecular level compared with their oxygen analogues.[31,32] A few exceptions include, for example, recent studies on monohydrated complexes of furfuryl mercaptan and furfuryl alcohol,[33] thenyl mercaptan (TM) and thenyl alcohol (TA),[34] trimethylene oxide and trimethylene sulfide,[14] and thiophene[13] by rotational spectroscopy

which have helped to fill this gap. These studies showed that the electronic properties of the chalcogen atom (O or S) plays a major role both in the conformational stabilities of the organic compound, and in the preferred binding sites for water and internal dynamics of the complex. The thiophene-water dimer, for instance, is formed by the water molecule binding primarily to the π-electrons of the ring, while in the furan-analogue[35] water interacts preferentially with the oxygen atom of the ring. Furthermore, tunneling splittings were observed in the rotational spectrum of the ground state structures of both complexes due to internal motions of water within the clusters. In thiophene-water, where the sulfur HB is weaker, a highly averaged structure was observed with water situated over the ring nearly in the thiophene σ_v plane rather than off-center closer to one π-bond of the ring as in the equilibrium structure.[13] This was likely due to smaller energy barriers for the internal motions of water when bound to the π-system, although a comprehensive analysis on furan-water have not been reported to date for comparison.[36] For the TA and TM monohydrates, fundamental differences were observed in their binding topologies as water primarily acts as a HB acceptor in TA via a O–H···O_w HB and as a HB acceptor in TM through a O_w–H···S HB (where O_w refers to the oxygen from water). Both monohydrates are further stabilized from secondary O_w–H···π interactions between the water and the ring π-electrons.

While previous reports on O and S-containing dimers have focused on cyclic monomers rather than more flexible molecules,[13,14,33,34,37–42] it is valuable to explore the conformational landscape of larger compounds with more diverse conformer distributions. Such studies would provide key information on how binding with a partner such as water impacts the conformer distribution of the monomer systems. This has been demonstrated

previously in the case of allylmethylamine-water,[8] for example, where the interaction with water was sufficient to re-order the relative stabilities of conformers compared to the ordering of the isolated monomers. To build on this, diallyl ether (DAE)[43] and diallyl sulfide (DAS)[43] are chosen as model systems in the present work as we recently reported surprising differences in the competitive nature of their conformational landscapes using rotational spectroscopy. Although both species have similar arrangements of the allyl sidechains in their ground state structures, the rotational spectrum of DAE exhibited transitions from nine low-energy conformers while for DAS, features due to only the lowest energy conformer were observed. With addition of a single water molecule, we are interested in investigating how the conformational equilibrium of ethers and sulfides are modified in the presence of intermolecular interactions and how the nature of the chalcogen binding partner influences the strength and topology of the interactions.

In this paper, we explore the conformational landscapes of the DAE and DAS monohydrates, DAE-w and DAS-w, using Fourier transform microwave (FTMW) spectroscopy and quantum chemistry calculations. Rotational transitions arising from the global minimum of each complex were observed and successfully assigned. Tunneling splittings associated with internal motions of water were observed for the DAS-w transitions which provides experimental evidence of a weaker HB interaction through its influence on the barrier to the water internal motions. Quantum theory of atoms in molecules (QTAIM), noncovalent interaction (NCI) analyses and symmetry-adapted perturbation theory (SAPT) calculations provide deeper understanding of the unique interactions responsible for the stability of the monohydrates of DAE and DAS.

Experimental Methods

The rotational spectra of DAE-w and DAS-w were collected using a broadband chirped pulse (8–18 GHz) and a cavity based Balle-Flygare (6–19 GHz) Fourier transform microwave (FTMW) spectrometer. The technical details and operating principles of each instrument have been described in detail elsewhere.[44,45] To produce the monohydrated complexes, a gas mixture containing ~1% of DAE or DAS vapour from a room temperature liquid sample was seeded in Ne and bubbled through a reservoir containing water. The resultant mixture was inserted into the high vacuum chamber of the instruments via a pulsed solenoid valve (1 mm diameter orifice) creating a supersonic jet. Initially, survey spectra from 8–18 GHz were recorded in segments of 2 GHz each using the chirped pulse FTMW instrument. For each measurement, a total of one million free induction decays (FIDs) were collected and averaged. In the broadband spectra, the most intense transitions of the monohydrates were readily identified leading to preliminary assignments. Next, the assignments were confirmed by additional measurements using the cavity-based spectrometer which features higher resolution and sensitivity allowing less intense lines to be recorded and small splittings to be resolved. Spectral lines recorded using the cavity-based instrument appear as Doppler doublets due to the instrument setup in which the molecular beam and resonator axis are collinear. Observed line widths for transitions measured with the BF-FTMW instrument are usually ~7 kHz (FWHM) and the uncertainty in assigning the line positions is about ± 2 kHz.

Computational Methods

In our study of the DAE and DAS monomers, transitions from nine stable conformers of DAE were observed in the rotational spectrum while only spectral signatures for the global minimum of DAS were detected.[43] Since the inclusion of a water molecule to form the monohydrated complexes may disrupt intramolecular interactions occurring in the monomers and alter their relative energy orderings, a comprehensive conformational search for DAE-w and DAS-w was needed for all possible orientations of the monomer geometries and interaction sites for the water molecule. Initial conformational searches for the energy minima of DAE-w and DAS-w were carried out at the GFN2-xTB[46] level of theory using the iMTD-GC algorithm of the conformer-rotamer ensemble sampling tool (CREST) available in the extended tight binding (xTB)[47,48] program package. During the searches, the possible geometries of the DAE and DAS monomers and binding sites for the water molecule were automatically considered by CREST. The automated search yielded 137 and 25 possible geometries for DAE-w and DAS-w, respectively. These geometries were then fully optimized using density functional theory (DFT) B3LYP[49]-D3(BJ)[50,51] with Dunning's aug-cc-pVTZ[52] basis set. These calculations identified 78 and 15 distinct minima for DAE-w and DAS-w, respectively. It is noteworthy that certain initial geometries from CREST exhibited unusual orientations (e.g. water subunit extremely distant from the monomers) and did not converge. Additionally, numerous geometries converged to the same minima after being optimized at the higher level of theory, which further reduced the number of conformers. To verify the nature of the stationary points and to calculate electronic energies with zero-point corrections (ZPE) as well as quartic centrifugal distortion constants, vibrational frequency

calculations were carried out within the harmonic approximation at the same levels of theory. All optimization and harmonic frequency calculations were performed using the Gaussian 16[53] program with the inclusion of Boys and Bernardi's counterpoise method[54] in all calculations to address the basis set superposition (BSSE) error.

As conformers with relative energies larger than 6 kJ mol^{-1} are not expected to be sufficiently populated in the supersonic jet based on the performed calculations, we focused on the energy minima located within 6 kJ mol^{-1} of the global minimum for further consideration. In total, 22 and three stable conformers were found within this energy window for DAE-w and DAS-w (Table 1 and Figure 1), respectively, at the B3LYP-D3(BJ)/aug-cc-pVTZ level using this approach. Given that many conformers of DAE-w were close in energy, we also performed optimization calculations for the conformers of DAE-w and DAS-w from Table 1 using the double-hybrid B2PLYP-D3(BJ) method with the aug-cc-pVTZ basis set to confirm the conformer geometries and their relative electronic energies. The results for this second method are compiled as supplementary information.

To confirm the dramatic differences observed in the conformational landscapes of DAE-w and DAS-w, we performed additional optimization and frequency calculations at the B3LYP-D3(BJ)/aug-cc-pVTZ level in which the oxygen atom in the 22 low energy structures of DAE-w was replaced by sulfur. This identified 15 higher conformers of DAS-w with relative energies ranging from 6.4 to as high as 21.9 kJ mol^{-1} and one additional conformer that is 5.8 kJ mol^{-1} higher than the global minimum. A complete list of the relative energies and rotational parameters of all conformers is given in the supplementary material while the relative energies and spectroscopic parameters for the

most significant conformers of each complex, within 6 kJ mol^{-1} of the global minimum, are compiled in Table 1. Their geometries are depicted in Figure 1. The Cartesian coordinates corresponding to each of these minima are given in Tables S1-S26 of the Supplementary Material file.

To better understand the observed spectral patterns for DAE-w and DAS-w, additional optimization and vibrational frequency calculations were carried out at the B3LYP-D3(BJ)/aug-cc-pVTZ level to find possible transition state structures consistent with the internal motion of water within the complex to interconvert the two hydrogen atoms. Furthermore, post-optimization calculations were conducted to elucidate the intermolecular forces responsible for the most stable conformers of the monohydrates using non-covalent interaction (NCI)[55], quantum theory of atoms in molecules (QTAIM),[56] and symmetry-adapted perturbation theory (SAPT)[57] methods. These analyses were conducted using the NCIPLOT,[58] AIMALL[59] and Psi4[60] programs, respectively and were performed on the equilibrium structures obtained at the B3LYP-D3(BJ)/aug-cc-pVTZ level. For the energy decomposition SAPT analysis, we used the higher order SAPT2+(3)δMP2 method, also with the aug-cc-pVTZ basis set, which has been shown to provide more accurate interaction energies.[60]

Table 1. Calculated energies and spectroscopic parameters for the conformers of DAE-w and DAS-w within 6 kJ mol^{-1} at the B3LYP-D3(BJ)/aug-cc-pVTZ level of theory.

DAE-w	ΔE_0[a]	A/B/C[b]	$\lvert\mu_a\rvert$/ $\lvert\mu_b\rvert$/ $\lvert\mu_c\rvert$[c]
I	0.0	2071/1248/881	2.1/0.1/0.9
II	0.8	2501/1122/888	0.2/2.5/0.5
III	1.0	2279/1082/889	0.7/2.1/0.3
IV	1.4	2248/1070/825	0.1/1.8/1.0
V	2.3	2432/1060/812	1.3/2.5/0.6
VI	2.3	2585/1021/850	1.0/2.2/0.5
VII	2.6	1928/1263/885	1.7/1.1/0.3
VIII	2.6	2423/1010/762	0.9/2.6/0.1
IX	2.6	2015/1087/744	1.7/2.0/0.7
X	2.7	2995/920/750	1.0/2.1/0.1
XI	2.9	2664/924/737	0.0/2.4/0.6
XII	3.1	2121/1203/891	1.7/1.5/1.3
XIII	3.3	2755/1035/874	1.0/2.0/0.4
XIV	3.4	2080/1274/915	1.2/2.1/1.0
XV	3.5	2389/1148/997	0.9/2.7/0.3
XVI	3.6	3148/944/775	0.9/1.9/0.0
XVII	3.9	2804/1036/847	1.0/3.0/0.0
XVIII	4.4	1823/1263/838	1.6/1.9/0.0
XIX	4.8	2305/1147/919	0.5/2.4/0.9
XX	4.8	2148/1241/925	1.5/1.8/0.6
XXI	4.8	2196/1148/816	0.7/2.1/0.2
XXII	5.3	2341/1177/981	0.4/3.2/0.7
DAS-w	ΔE_0[a]	A/B/C[b]	$\lvert\mu a\rvert$/ $\lvert\mu b\rvert$/ $\lvert\mu c\rvert$[c]
I	0.0	1764/1042/814	1.4/0.4/0.5
II	5.8	1758/925/805	0.0/1.3/0.4
III	5.9	1824/911/738	0.6/0.4/0.4

[a]Zero-point energy (ZPE) corrected relative energies in kJ mol^{-1}, [b]Rotational constants in MHz, [c]Magnitude of the electric dipole moment components in Debye.

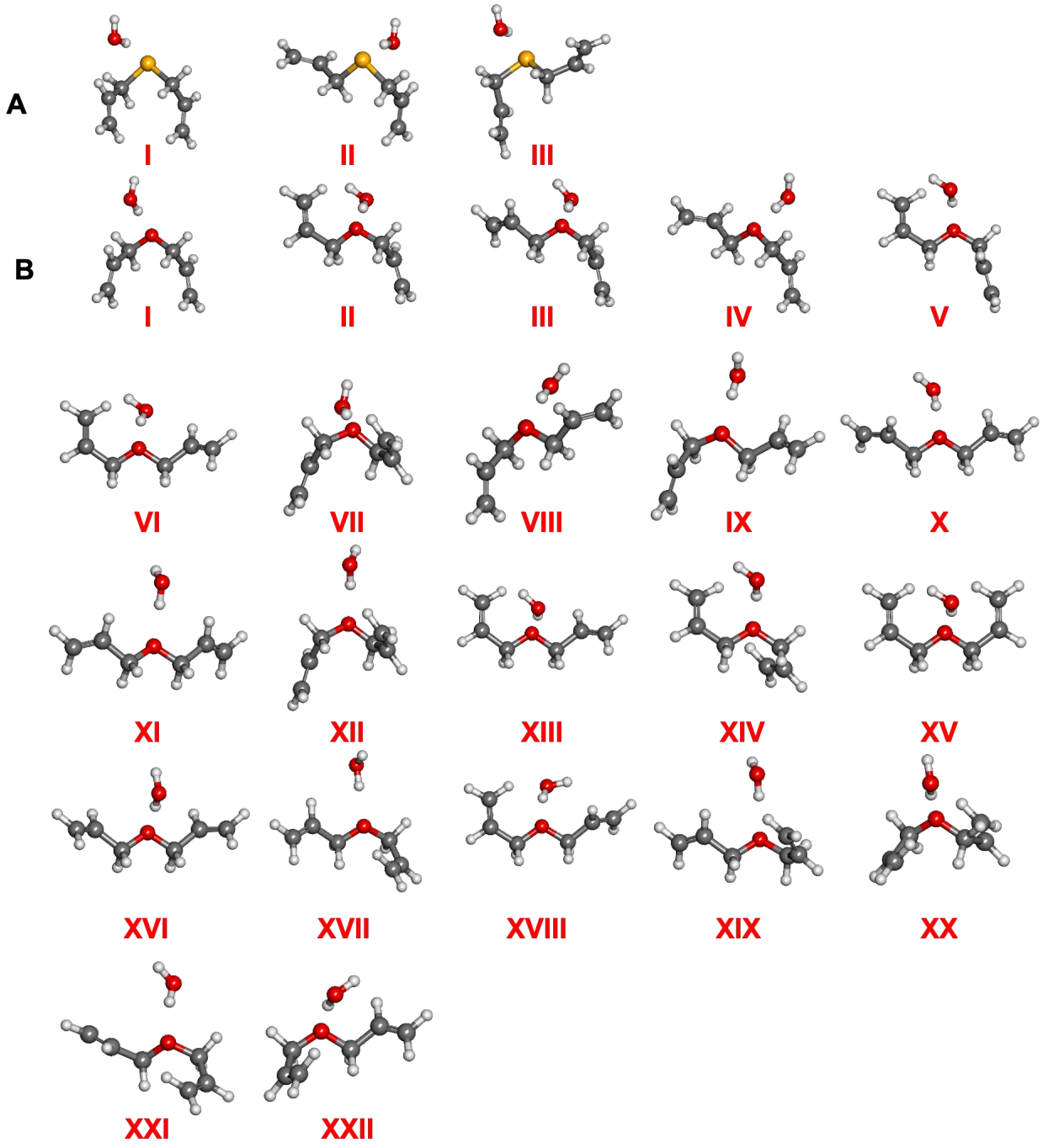

Figure 1. Minima energy conformers within 6 kJ mol^{-1} of the global minimum of A) DAS-w and B) DAE-w at the B3LYP-D3(BJ)/aug-cc-pVTZ level of theory.

Results

The calculated spectroscopic and energy parameters for stable complexes within 6 kJ mol^{-1} (B3LYP-D3(BJ)/aug-cc-pVTZ) of the global minimum of DAE-w and DAS-w are provided in Table 1 and the geometries are displayed in Figure 1. Roman numerals were used to label the stability ordering of conformers from B3LYP-D3(BJ), with conformer I being the most stable geometry. Comparison with the results from the B2PLYP-D3(BJ) method, given as supplementary material using the same conformer labels, reveal that the same conformational equilibrium is captured by both methods although in some cases, the relative energy orderings change for DAE-w conformers. This is not surprising given the highly competitive conformational landscape of this complex.

Experimentally, after subtracting transitions from the parent and singly-substituted isotopologues of the DAE and DAS monomers as well as known lines due to the water dimer, an additional set of transitions were observed in the broadband spectrum of each gas mixture. The observed patterns were consistent with those predicted for the most stable conformers of DAE-w-I and DAS-w-I in Table 1. With the high-resolution of the BF-FTMW instrument, a tunnelling splitting was detected in the spectrum of DAS-w-I, an example of which is shown in Figure 2. The splitting components present a typical 3:1 ratio of intensities related to the ortho-para nuclear spin statistics for exchange of two hydrogen atoms. No resolvable splittings were observed in the transitions of DAE-w-I. In total, 48 *a*-type and 21 *c*-type rotational transitions were observed for DAE-w-I. The observed types of transitions align well with the calculated dipole moment components (Table 1). No *b*-type transitions were detected for DAE-w as the predicted value of μ_b is small. For DAS-w, 49 *a*-type and two *b*-type transitions were observed for the most

intense tunneling component, whereas 40 *a*-type and one *b*-type transition were seen for the other component due to its less intense transitions. Although the absolute values predicted for μ_b= 0.4 D and μ_c= 0.5 D are similar, no *c*-type transitions could be observed for DAS-w-I. The absence of *c*-type transitions in the spectrum of DAS-w-I provide a clue to identify the tunneling motion associated with the water dynamics that averages out along the dimer c-axis.

All rotational transitions observed for conformer I of DAE-w and DAS-w were fit using Pickett's SPFIT program[61] (Watson's S-reduced Hamiltonian, I^r representation) to derive experimental rotational and quartic centrifugal distortion constants. The resulting parameters are given in Table 2, while the transition frequencies are listed in Tables S28-S30. The two tunneling states observed for DAS-w-I were analyzed independently and are labeled in Table 2 as I+ and I-. It is worth noting that although DAE-w is predicted to have a more competitive equilibrium with many other low energy conformers (Table 1), only lines due to the global minimum conformer I could be assigned. After removing lines from all detected species, many low intensity features remain in the DAE-w spectra which may arise from other conformers of DAE-w or from higher-order hydrates, however, no convincing assignment was achieved.

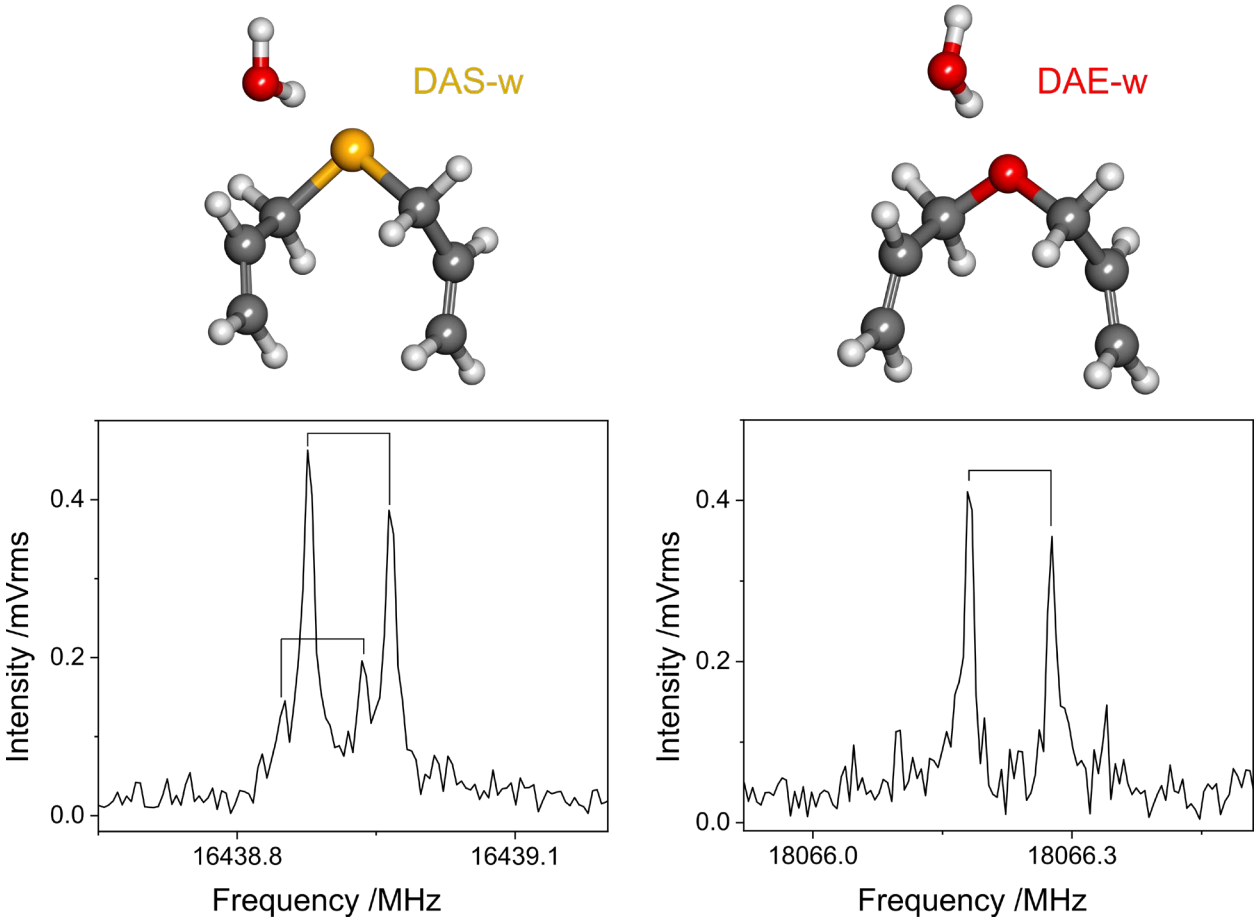

Figure 2. Equilibrium structures (B3LYP-D3(BJ)/aug-cc-pVTZ) and BF-FTMW spectra of the $10_{1,10}$–$9_{1,9}$ rotational transitions of conformer I of DAS-w (left) and DAE-w (right).

Table 2. Ground state spectroscopic parameters for the observed conformers of DAE-w and DAS-w including the two tunnelling states for DAS-w.

Parameter	DAE-w	DAS-w	
	I	I+	I-
A/MHz[a]	2109.51322(23)	1774.0279(24)	1774.0327(28)
B/MHz	1223.563388(88)	1021.31707(20)	1021.31552(24)
C/MHz	870.307757(72)	799.01585(13)	799.01393(13)
D_J/kHz[b]	0.64402(59)	1.7555(11)	1.7525(20)
D_{JK}/kHz	2.1011(40)	-11.264(15)	-11.265(18)
D_K/kHz	5.814(12)	26.25(17)	26.42(24)
d_1/kHz	-0.12870(37)	0.06985(57)	0.0702(11)
d_2/kHz	-0.07005(20)	-0.02091(47)	-0.02136(46)
$\mu_a/\mu_b/\mu_c$[c]	y/n/y	y/y/n	y/y/n
N[d]	69	51	41
σ/kHz[e]	1.5	2.2	1.9

[a]Rotational constants; [b]quartic centrifugal distortion constants; [c]electric dipole moment components ("y" if observed and "n" if not observed); [d]total number of lines in the fit; [e]root-mean-square deviation of the fit. A complete list of calculated parameters at the B3LYP-D3(BJ)/aug-cc pVTZ level of theory is provided in Table S27 for comparison.

Discussion

In the presence of a single water molecule, the overall conformational landscapes of the DAE and DAS monomers remain surprisingly different as DAE-w is predicted to form many low energy conformers whereas DAS-w adopts only one particularly stable geometry (Table 1). For the lowest energy of forms of each monohydrate (Conformer I), the ether and sulfide geometries closely match those previously reported for the isolated DAE[43] and DAS[43] monomers (Appendix 8 of supplementary material) with dihedral angles describing the heavy atom backbone maintained to within two degrees. Although the

geometries themselves are not significantly altered, the relative stabilities of conformers beyond the global minimum change following complexation with water, particularly for DAE (Table 1). This is exemplified, for example, by the destabilization of conformer II of DAE,[43] which becomes only the fifteenth most stable dimer, conformer XV of DAE-w (Table 1), indicating that interactions with water disrupt the conformational equilibrium of DAE. Specifically, conformer II of DAE adopts a W-shaped structure, stabilized by orbital LP(O) → $\sigma^*_{C\text{-}C}$ interactions involving the lone-pairs on oxygen and the allyl side chains.[43] Upon binding to water in DAE-w, these intramolecular interactions in the monomer are diminished as now the central oxygen atom of DAE also binds to the water subunit leading to the higher energy of DAE-w conformer XV (Figure 1). A similar effect is also observed for DAE conformer IV, that exhibits a V-shaped structure (only one allyl side chain pointing up) and is destabilized upon binding with water to form the DAE-w conformer XIII (Figure 1). This does not extend to every V- or W-shaped structure of the monomers, however, as the second most stable dimer, DAE-w-II, has a V-shaped arrangement within the organic framework and corresponds to conformer III of the DAE monomer. This indicates that there are more effects at play and that the stabilization of the dimers also depends on the orientation of the other allyl group on the opposite side and how it interacts with water. From these examples of the effect of water on the relative stabilities of the monomer structures, it is evident that the orbital interactions involving the lone-pairs on the chalcogen are central to stabilizing the monomer geometries that give rise to its highly competitive conformational equilibria.[43] These intramolecular contacts appear even more important than in the case of the allylmethylamine monohydrate (AMA-w) dimer,[8] in which binding to water only disrupted the relative energy ordering of the higher energy forms of

AMA while in DAE-w and DAS-w, the conformational stabilities are altered for most complexes beyond the global minimum geometries.

As shown in Figure 1, in all low energy geometries of DAE-w and DAS-w , water binds preferentially to the central chalcogen atom through a OH···X (X= O, S) HB. Additionally, secondary HBs between the oxygen of water and the allyl substituents become possible due to the favourable orientation of these groups within most isomers. To gain a deeper understanding of the topology of the interactions present in the observed conformers of DAE-w and DAS-w, we carried out NCI analyses and the outcomes are illustrated in Figure 3. The NCI isosurfaces of both clusters are similarly placed and confirm the presence of both primary and secondary HBs with the strongest contact being the intermolecular OH···X (X= O, S) interaction (blue isosurface). For a quantitative comparison of the HB strengths, we analyzed in detail NCI plots of reduced density gradient (RDG) values against the sign of the second eigenvalue of the electron density Hessian matrix $\text{sign}(\lambda_2)\rho$, which can also distinguish between attractive ($\lambda_2 < 0$) and repulsive ($\lambda_2 > 0$) interactions.[55,58] In these plots, the primary HB is identified by the most negative peak, and it is evident from the figure that the sulfur contact ($\text{sign}(\lambda_2)\rho \sim -0.02$) is weaker than the oxygen one ($\text{sign}(\lambda_2)\rho \sim -0.03$). The secondary CH···O HB, represented by the negative peak around $\text{sign}(\lambda_2)\rho \sim -0.01$ for both clusters, is slightly stronger in DAS-w. Additional support of the NCI findings is obtained from QTAIM molecular graphs (Figure S1 and Table S31) which show the presence of a bond critical point (BCP) between the atoms involved in the HB interactions. The QTAIM results confirm the nature of the primary and secondary HBs with the primary contact being considerably smaller in DAS-w (-16.7 kJ mol^{-1}) than in DAE-w (-36.7 kJ mol^{-1}) but the secondary interaction

showing the reverse trend (-5.0 kJ mol^{-1} versus -3.5 kJ mol^{-1} for DAS-w and DAE-w, respectively). The magnitude of the interactions is consistent with the bond lengths between the participating atoms from the equilibrium structures at the B3LYP-D3(BJ)/aug-cc-pVTZ level (OH···O= 1.86 Å and CH···O= 2.79 Å in DAE-w, and OH···S= 2.39 Å and CH···O= 2.59 Å in DAS-w). Apart from the HBs with water, the NCI graphs also exhibit weak intramolecular contacts (either attractive or repulsive) between the allyl moieties in DAE and DAS shown as green isosurfaces in Figure 3. These interactions were also observed in the NCI graphs of the corresponding monomers in the absence of water indicating that binding with water does not significantly alter the intramolecular contacts in these geometries.

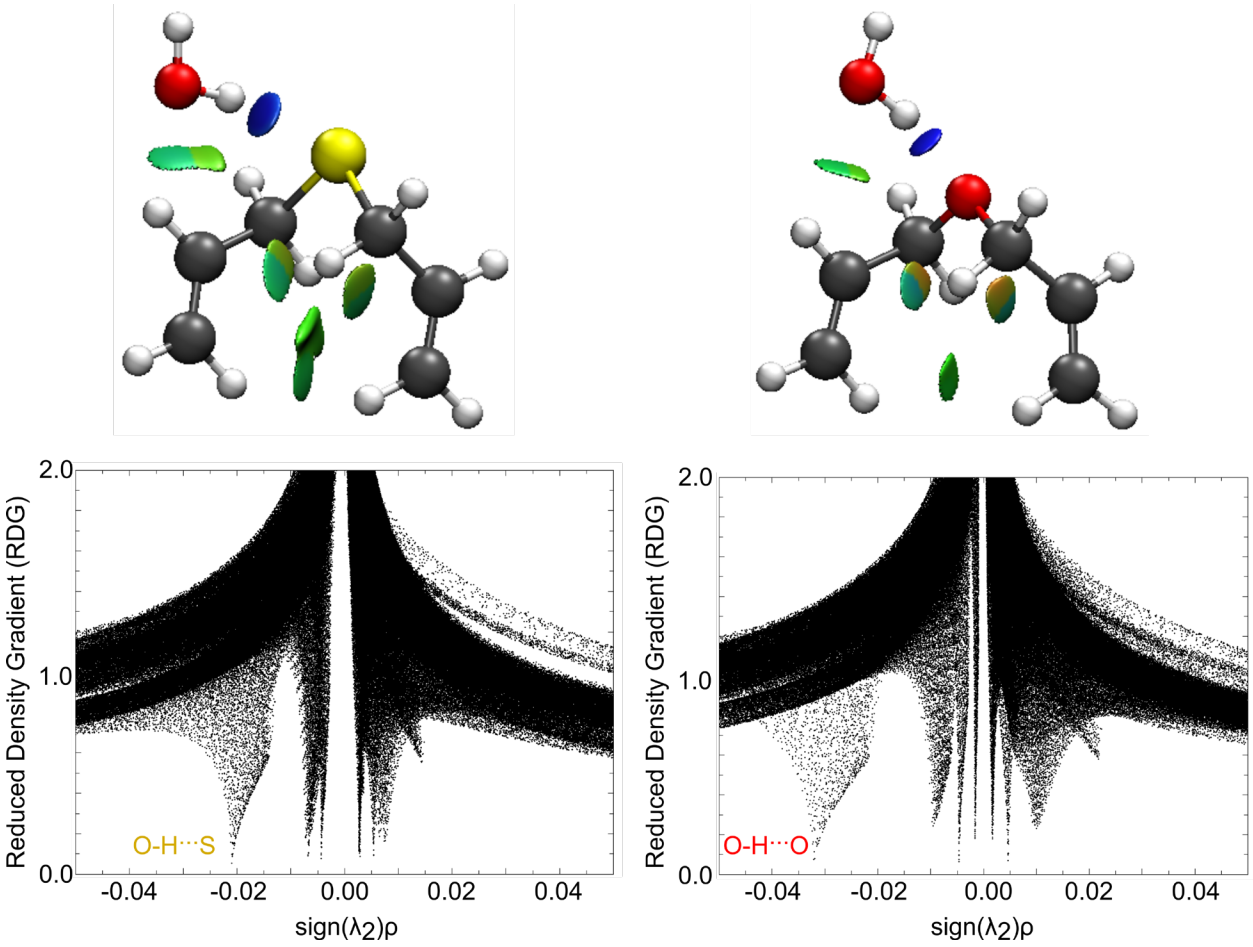

Figure 3. NCI isosurface (top) and graphs of reduced density gradient (RDG) versus sign(λ_2)ρ (bottom) for conformer I of DAS-w (left) and DAE-w (right).

The nature of the intermolecular HBs was further investigated using symmetry-adapted perturbation theory (SAPT) calculations at the SAPT2+(3)δMP2/aug-cc-pVTZ level of theory, shown in Figure 4. The total SAPT energy for DAE-w and DAS-w are -27.9 kJ mol^{-1} and -21.2 kJ mol^{-1}, respectively, in agreement with the DFT interaction energies (-28.7 kJ mol^{-1} for DAE-w and -23.5 kJ mol^{-1} for DAS-w), which are the energy difference between the product complex and its monomer components accounting also for the BSSE error and ZPE corrections. Decomposing the overall SAPT energy into the three stabilizing components (electrostatics, induction, and dispersion) and the one

destabilizing exchange-repulsion component reveals that the electrostatic portion is the most significant contributor to the stabilization of both DAE-w and DAS-w, followed by dispersion and induction effects. Upon chalcogen substitution from DAE-w to DAS-w, there is an increase of approximately 7% in the contribution from dispersion, which aligns well with the knowledge that sulfur HBs are more dispersive in nature than oxygen HBs due to the weaker HB acceptor character of sulfur.

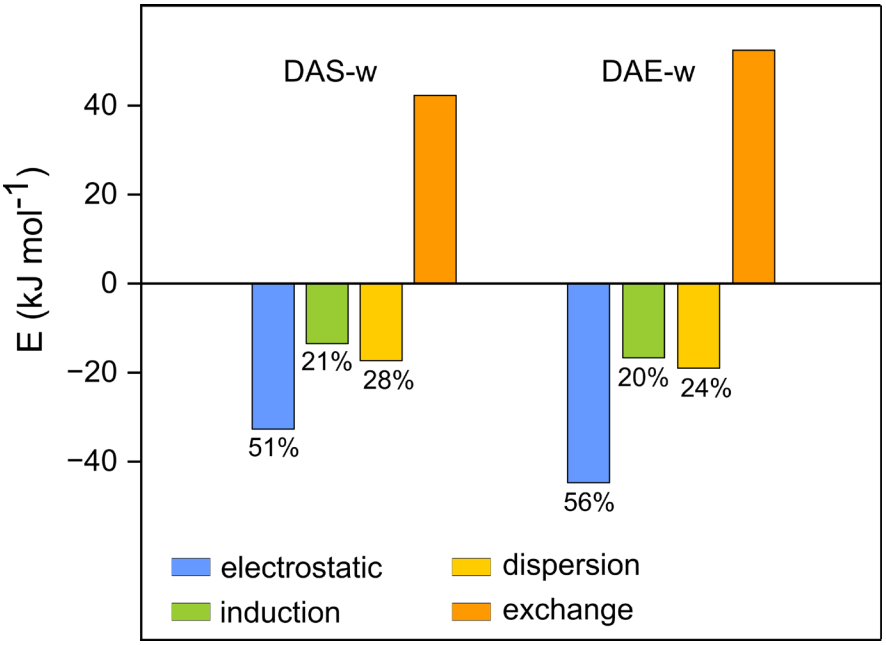

Figure 4. Histogram of the stabilizing (electrostatic, induction, dispersion) and destabilizing exchange-repulsion components of the total SAPT interaction energy of DAS-w (-21.2 kJ mol^{-1}) and DAE-w (-27.9 kJ mol^{-1}). The percentages represent the contribution of that specific term to the total stabilizing energy (electrostatic + induction + dispersion). The values of each term are provided in Table S32.

Finally, to further explore how the HB strengths contribute to the distinct energy barriers associated with the internal motions of water, we identified and optimized transition state (TS) structures for potential tunneling pathways for each complex at the

B3LYP-D3(BJ)/aug-cc-pVTZ level. During the TS search, we focused on pathways that would lead to exchange of the protons of water as the observed tunneling for DAS-w shows a typical 3:1 ratio (Figure 2) of intensities as one would expect based on ortho-para nuclear spin statistics for exchange of two hydrogen atoms. The possible TS structures identified for DAS-w and DAE-w are given in Figure 5 and their Cartesian coordinates are provided in Tables S33 and S34, respectively. For each, we found a vibrational imaginary frequency linked to a motion which interconverts the hydrogen atom of water that binds to the central chalcogen atom. Notably, the position of water in the TS structures for DAE-w and DAS-w are significantly different. In the DAE-w TS, the water molecule is positioned near the lone pairs of the ether oxygen with both hydrogen atoms approximately 2.4 Å from the bridge atom and its C_{2V} axis slightly tilted toward one of the allyl groups. This is likely a consequence of the disruption to the primary HB making the water molecule adopt a slightly more favourable location. In contrast, in the DAS-w TS, the water subunit remains on one side of the molecule closer to one allyl fragment but now positions one hydrogen atom facing the sulfur, while the other hydrogen is oriented towards the allyl side chain. The difference in the TS geometries likely reflects the dominance of the primary HB interaction in DAE-w and its greater electrostatic nature in comparison to DAS-w whereas in the latter, the secondary interaction between water and the allyl group is sufficiently strong to maintain the interaction between these groups in the TS. The tunneling motion in DAS-w occurs through a TS barrier of 6.0 kJ mol^{-1} accounting for zero-point corrections, while the analogous barrier in DAE-w is 9.4 kJ mol^{-1} which are consistent with the strength of the S and O HBs that are disrupted during the water internal motion. This barrier difference of 3.4 kJ mol^{-1} is sufficient to prevent the

observation of tunneling splittings for DAE-w in our frequency range given that the tunneling components were barely-resolved for DAS-w (Figure 2).

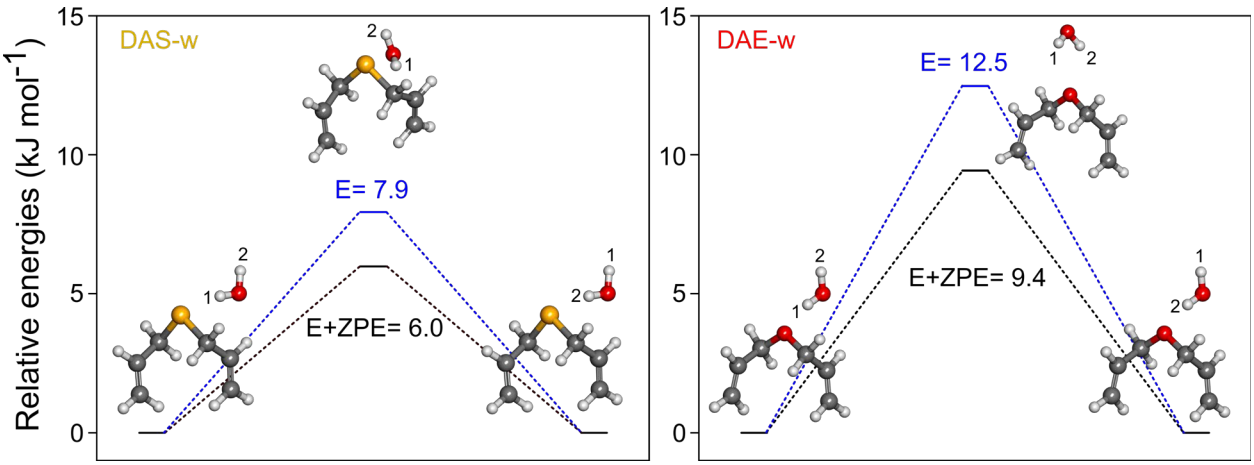

Figure 5. Possible transition states for the water internal motion within the DAE-w (left) and DAS-w (right) that have a vibrational imaginary frequency consistent with a motion of water that leads to the exchange of the water protons.

Conclusions

The powerful combination of rotational spectroscopy and quantum chemistry calculations has provided insights into the impact of a single water molecule on the conformational landscape of DAE and DAS at the molecular level. Compared to the ring monohydrate analogues like thiophene-water[13] and furan-water,[35,36] as well as thenyl alcohol-water[34] and thenyl mercaptan-water,[34] where the binding sites are different for the O and S congeners, the investigation of the DAE-w and DAS-w conformational landscapes shows that the overall topology of the intermolecular interaction with water is more similar for the two species. On closer inspection, however, the binding to water disrupts the stability ordering of the flexible monomer backbones in both DAE and DAS

which speaks to the importance of the intramolecular orbital interactions involving the LP(O) and LP(S) in stabilizing the associated monomer systems. Differences in the HB acceptor character of O and S also lead to unique features in the spectra of these complexes with the weaker binding between water and DAS giving rise to a more dynamic complex. In summary, our study demonstrates how the nature of the chalcogen atom in large and flexible monomers affects their interactions with binding partner molecules and impacts their conformational equilibria. Characterizing these features at the molecular level fosters novel insights into solvation processes and internal dynamics of organic ethers and sulfides.

Supplementary Material

Appendix 1: Cartesian coordinates for the energy minima of DAS-w and DAE-w; Appendix 2: Calculated energetic and spectroscopic parameters for conformer I of DAS-w and DAE-w; Appendix 3: Assigned transitions for the observed species of conformer I of DAS-w and DAE-w; Appendix 4: QTAIM parameters and molecular graphs for conformer I of DAS-w and DAE-w; Appendix 5: Symmetry-adapted perturbation theory results of DAS-w and DAE-w; Appendix 6: Cartesian coordinates of the transition state structures of DAE-w and DAS-w; Appendix 7: Calculated energies and parameters for conformers of DAE-w and DAS-w at B2PLYP-D3(BJ)/aug-cc-pVTZ and B3LYP-D3(BJ)/aug-cc-pVTZ levels; Appendix 8: Comparison between the monomers and monohydrates of DAE and DAS.

Acknowledgments

This research is funded by the Natural Sciences and Engineering Research Council of Canada (NSERC) through the Discovery Grant program (JvW) and the high-performance computing facility (GREX) provided by the University of Manitoba and Digital Research Alliance of Canada. TP is supported by the Faculty of Graduate studies through a UM graduate fellowship (UMGF). WGDPS also acknowledges support from a UMGF during his time at the University of Manitoba.

Author Declarations

Conflict of Interest

The authors have no conflicts to disclose.

R*eferences*

[1] E. Brini, C.J. Fennell, M. Fernandez-Serra, B. Hribar-Lee, M. Lukšič, and K.A. Dill, "How Water's Properties Are Encoded in Its Molecular Structure and Energies," Chem. Rev. **117**(19), 12385–12414 (2017).

[2] G. Hummer, and A. Tokmakoff, "Preface: Special topic on biological water," J. Chem. Phys. **141**(22), 1–3 (2014).

[3] C.J. Li, and L. Chen, "Organic chemistry in water," Chem. Soc. Rev. **35**(1), 68–82 (2006).

[4] N. Nandi, K. Bhattacharyya, and B. Bagchi, "Dielectric relaxation and solvation dynamics of water in complex chemical and biological systems," Chem. Rev. **100**(6), 2013–2045 (2000).

[5] B. Bagchi, *Water in Biological and Chemical Processes: From Structure and Dynamics to Function* (Cambridge University Press, 2013).

[6] W. Sun, and M. Schnell, “Microhydrated 3-Methyl-3-oxetanemethanol: Evolution of the Hydrogen-Bonding Network from Chains to Cubes,” Angew. Chemie - Int. Ed. **61**(49), e202210819 (2022).

[7] W. Li, M.M. Quesada-Moreno, P. Pinacho, and M. Schnell, “ Unlocking the Water Trimer Loop: Isotopic Study of Benzophenone-$(H_2O)_{1–3}$ Clusters with Rotational Spectroscopy ,” Angew. Chemie **133**(10), 5383–5390 (2021).

[8] W.G.D.P. Silva, T. Poonia, and J. van Wijngaarden, “Exploring the non-covalent interactions behind the formation of amine-water complexes: The case of N-allylmethylamine monohydrate,” Phys. Chem. Chem. Phys. **23**(12), 7368–7375 (2021).

[9] P. Pinacho, J.C. López, Z. Kisiel, and S. Blanco, “Microsolvation of ethyl carbamate conformers: Effect of carrier gas on the formation of complexes,” Phys. Chem. Chem. Phys. **22**(33), 18351–18360 (2020).

[10] G. Salvitti, F. Baroncelli, C. Nicotri, L. Evangelisti, S. Melandri, and A. Maris, “How Water Interacts with the NOH Group: The Rotational Spectrum of the 1:1 N,N-diethylhydroxylamine·Water Complex,” Molecules **27**(23), 1–14 (2022).

[11] B. Wu, N.A. Seifert, S. Oswald, W. Jäger, and Y. Xu, “Rotational Spectroscopy of the 2,2,3,3,3-Pentafluoropropanol···Water Complex: Conformations and Large Amplitude Motions,” ChemPhysChem **23**(20), e202200348 (2022).

[12] B. Wu, A.S. Hazrah, N.A. Seifert, S. Oswald, W. Jäger, and Y. Xu, “Higher-Energy Hexafluoroisopropanol···Water Isomer and Its Large Amplitude Motions: Rotational Spectra and DFT Calculations,” J. Phys. Chem. A **125** (48), 10401–10409 (2021).

[13] W.G.D.P. Silva, and J. van Wijngaarden, “Characterization of Large-Amplitude Motions and Hydrogen Bonding Interactions in the Thiophene-Water Complex by Rotational Spectroscopy,” J. Phys. Chem. A **125**(16), 3425–3431 (2021).

[14] W.G.D.P. Silva, and J. van Wijngaarden, “Hydrogen bonding networks and cooperativity effects in the aqueous solvation of trimethylene oxide and sulfide rings by microwave spectroscopy and computational chemistry,” J. Chem. Phys. **155**(3), 034305 (2021).

[15] L. Ferres, L. Evangelisti, A. Maris, S. Melandri, W. Caminati, W. Stahl, and H.V.L. Nguyen, “Skeletal Torsion Tunneling and Methyl Internal Rotation: The Coupled Large Amplitude Motions in Phenyl Acetate,” Molecules **27**(9), 2730 (2022).

[16] H.V.L. Nguyen, W. Caminati, and J.U. Grabow, “The LAM of the Rings: Large Amplitude Motions in Aromatic Molecules Studied by Microwave Spectroscopy,” Molecules **27**(12), 3948 (2022).

[17] W. Cheng, Y. Zheng, G. Feng, J.U. Grabow, and Q. Gou, “Conformation and bonding of 2-methoxypyridine and its monohydrate from rotational spectra,” Spectrochim. Acta - Part A Mol. Biomol. Spectrosc. **239**, 118434 (2020).

[18] E. Arunan, G.R. Desiraju, R.A. Klein, J. Sadlej, S. Scheiner, I. Alkorta, D.C. Clary, R.H. Crabtree, J.J. Dannenber, P. Hobza, H.G. Kjaergaard, A.C. Legon, B. Mennucci, and D.J. Nesbitt, “Definition of the hydrogen bond (IUPAC Recommendations 2011),” Pure Appl. Chem. **83**(8), 1637–1641 (2011).

[19] A. Chand, D.K. Sahoo, A. Rana, S. Jena, and H.S. Biswal, “The Prodigious Hydrogen Bonds with Sulfur and Selenium in Molecular Assemblies, Structural Biology, and Functional Materials,” Acc. Chem. Res. **53**(8), 1580–1592 (2020).

[20] N.T. Bui, H. Kang, S.J. Teat, G.M. Su, C.W. Pao, Y.S. Liu, E.W. Zaia, J. Guo, J.L. Chen, K.R. Meihaus, C. Dun, T.M. Mattox, J.R. Long, P. Fiske, R. Kostecki, and J.J. Urban, “A nature-inspired hydrogen-bonded supramolecular complex for selective copper ion removal from water,” Nat. Commun. **11**(1), 1–12 (2020).

[21] S. Dai, L.M. Funk, F.R. von Pappenheim, V. Sautner, M. Paulikat, B. Schröder, J. Uranga, R.A. Mata, and K. Tittmann, “Low-barrier hydrogen bonds in enzyme cooperativity,” Nature **573**(7775), 609–613 (2019).

[22] R. Zhang, A. Khalizov, L. Wang, M. Hu, and W. Xu, “Nucleation and growth of nanoparticles in the atmosphere,” Chem. Rev. **112**(3), 1957–2011 (2012).

[23] J.U. Bowie, “Membrane protein folding: How important are hydrogen bonds?,” Curr. Opin. Struct. Biol. **21**(1), 42–49 (2011).

[24] T. Lu, J. Zhang, Y. Xu, Z. Wang, G. Feng, and Z. Zeng, “Hydrogen bond interactions between thioethers and amides: A joint rotational spectroscopic and theoretical study of the formamide···dimethyl sulfide adduct,” Spectrochim. Acta - Part A Mol. Biomol. Spectrosc. **288**, 122199 (2023).

[25] Y. Zheng, J. Chen, C. Duan, X. Zhang, X. Xu, and Q. Gou, “Accurate Geometry and Non-Covalent Interactions in 1-Phenylethanol and its Monohydrate: A Rotational Study,” ChemPhysChem **24**(7), 1–7 (2023).

[26] W. Li, M. Li, Y. Jin, Q. Gou, J.U. Grabow, and G. Feng, “Molecular structure and non-covalent interaction of 2-thiophenecarboxaldehyde and its monohydrated complex,” J. Chem. Phys. **151**(16), 164307 (2019).

[27] E.N. Baker, and R.E. Hubbard, “Hydrogen bonding in globular proteins,” Prog. Biophys. Mol. Biol. **44**(2), 97–179 (1984).

[28] T. Steiner, and G. Koellner, “Hydrogen bonds with π-acceptors in proteins: Frequencies and role in stabilizing local 3D structures,” J. Mol. Biol. **305**(3), 535–557 (2001).

[29] L. Jiang, and L. Lai, “CH···O hydrogen bonds at protein-protein interfaces,” J. Biol. Chem. **277**(40), 37732–37740 (2002).

[30] P. Zhou, F. Tian, F. Lv, and Z. Shang, “Geometric characteristics of hydrogen bonds involving sulfur atoms in proteins,” Proteins Struct. Funct. Bioinforma. **76**(1), 151–163 (2009).

[31] H.S. Biswal, *Hydrogen Bonding Involving Sulfur: New Insights from Ab Initio Calculations and Gas Phase Laser Spectroscopy* (in Noncovalent Forces, ed. S. Scheiner, Springer Int. Pub., Switzerland, 2015).

[32] H.S. Biswal, S. Bhattacharyya, A. Bhattacherjee, and S. Wategaonkar, “Nature and strength of sulfur-centred hydrogen bonds: Laser spectroscopic investigations in the gas phase and quantum-chemical calculations,” Int. Rev. Phys. Chem. **34**(1), 99–160 (2015).

[33] M. Juanes, A. Lesarri, R. Pinacho, E. Charro, J.E. Rubio, L. Enríquez, and M. Jaraíz, “Sulfur Hydrogen Bonding in Isolated Monohydrates: Furfuryl Mercaptan versus Furfuryl Alcohol,” Chem. - A Eur. J. **24**(25), 6564–6571 (2018).

[34] M. Juanes, R.T. Saragi, R. Pinacho, J.E. Rubio, and A. Lesarri, “Sulfur hydrogen bonding and internal dynamics in the monohydrates of thenyl mercaptan and thenyl alcohol,” Phys. Chem. Chem. Phys. **22**(22), 12412–12421 (2020).

[35] S.P. Lockwood, T.G. Fuller, and J.J. Newby, “Structure and Spectroscopy of Furan:H_2O Complexes,” J. Phys. Chem. A **122**(36), 7160–7170 (2018).

[36] F.L. Bettens, R.P.A. Bettens, and A. Bauder, “The Microwave Spectrum and r_0 Structure of the Furan···H_2O Complex, A Case of Large Amplitude Motion,” Int. Symp.

Mol. Spectrosc., (1994).

[37] J.L. Alonso, S. Antolínez, S. Blanco, A. Lesarri, J.C. López, and W. Caminati, “Weak C-H···O and C-H···F-C Hydrogen Bonds in the Oxirane-Trifluoromethane Dimer,” Acta Crystallogr. Sect. C Struct. Chem. **74**(12), 1610–1621 (2018).

[38] E.J. Cocinero, R. Sánchez, S. Blanco, A. Lesarri, J.C. López, and J.L. Alonso, “Weak hydrogen bonds C-H···S and C-H···F-C in the thiirane-trifluoromethane dimer,” Chem. Phys. Lett. **402**(1–3), 4–10 (2005).

[39] S. Antolínez, J.C. López, and J.L. Alonso, “Rotational spectra and structure of the hydrogen-bonded complex oxetane HCl,” Chem. Phys. Lett. **334**(4–6), 250–256 (2001).

[40] M.E. Sanz, J.C. López, and J.L. Alonso, “Axial and equatorial hydrogen-bond conformers and ring-puckering motion in the trimethylene sulfide-hydrogen fluoride complex,” Chem. - A Eur. J. **8**(18), 4265–4271 (2002).

[41] M.E. Sanz, V.M. Sanz, J.C. López, and J.L. Alonso, “Oxetane-hydrogen fluoride complex: A rotational study,” Chem. Phys. Lett. **342**(1–2), 31–38 (2001).

[42] M.E. Sanz, A. Lesarri, J.C.L. Pez, and J.L. Alonso, “Hydrogen bond in molecules with large-amplitude motions: A rotational study of trimethylene sulfide···HCl,” Angew. Chemie - Int. Ed. **40**(5), 935–938 (2001).

[43] T. Poonia, W.G.D.P. Silva, and J. van Wijngaarden, “Dramatic differences in the conformational equilibria of chalcogen-bridged compounds: The case of diallyl ether versus diallyl sulfide,” Phys. Chem. Chem. Phys. **24**(1), 240–248 (2022).

[44] L. Evangelisti, G. Sedo, and J. van Wijngaarden, “Rotational Spectrum of 1,1,1-Trifluoro-2-butanone Using Chirped-Pulse Fourier Transform Microwave Spectroscopy,” J. Phys. Chem. A **115**(5), 685–690 (2011).

[45] G. Sedo, and J. van Wijngaarden, “Fourier transform microwave spectra of a ‘new’ isomer of OCS-CO_2,” J. Chem. Phys. **131**(4), 044303 (2009).

[46] C. Bannwarth, S. Ehlert, and S. Grimme, “GFN2-xTB - An Accurate and Broadly Parametrized Self-Consistent Tight-Binding Quantum Chemical Method with Multipole Electrostatics and Density-Dependent Dispersion Contributions,” J. Chem. Theory Comput. **15**(3), 1652–1671 (2019).

[47] S. Grimme, “Exploration of Chemical Compound, Conformer, and Reaction Space with Meta-Dynamics Simulations Based on Tight-Binding Quantum Chemical Calculations,” J. Chem. Theory Comput. **15**(5), 2847–2862 (2019).

[48] P. Pracht, F. Bohle, and S. Grimme, “Automated exploration of the low-energy chemical space with fast quantum chemical methods,” Phys. Chem. Chem. Phys. **22**(14), 7169–7192 (2020).

[49] A.D. Becke, “A new inhomogeneity parameter in density-functional theory,” J. Chem. Phys. **109**(6), 2092–2098 (1998).

[50] S. Grimme, S. Ehrlich, and L. Goerigk, “Effect of the damping function in dispersion corrected density functional theory,” J. Comput. Chem. **32**(7), 1456–1465 (2011).

[51] S. Grimme, J. Antony, S. Ehrlich, and H. Krieg, “A consistent and accurate ab initio parametrization of density functional dispersion correction (DFT-D) for the 94 elements H-Pu,” J. Chem. Phys. **132**(15), 1–19 (2010).

[52] T.H. Dunning, “Gaussian basis sets for use in correlated molecular calculations. I. The atoms boron through neon and hydrogen,” J. Chem. Phys. **90**(2), 1007–1023 (1989).

[53] M.J. Frisch, G.W. Trucks, H.B. Schlegel, G.E. Scuseria, M.A. Robb, J.R. Cheeseman, G. Scalmani, V. Barone, B. Mennucci, G.A. Petersson, H. Nakatsuji, M. Caricato, X. Li,

H.P. Hratchian, A.F. Izmaylov, J. Bloino, G. Zheng, J.L. Sonnenberg, M. Hada, M.E. Fukuda, K. T. R., J. Hasegawa, M. Ishida, T. Nakajima, Y. Honda, O. Kitao, H. Nakai, T. Vreven, J.A. Montgomery, J.E. Peralta, F. Ogliaro, M. Bearpark, J.J. Heyd, E. Brothers, K.N. Kudin, V.N. Staroverov, R. Kobayashi, J. Normand, K. Raghavachari, A. Rendell, J.C. Burant, S.S. Iyengar, J. Tomasi, M. Cossi, N. Rega, J.M. Millam, M. Klene, J.E. Knox, J.B. Cross, V. Bakken, C. Adamo, J. Jaramillo, R. Gomperts, R.E. Stratmann, O. Yazyev, A.J. Austin, R. Cammi, C. Pomelli, J.W. Ochterski, R.L. Martin, K. Morokuma, V.G. Zakrzewski, G.A. Voth, P. Salvador, J.J. Dannenberg, S. Dapprich, A.D. Daniels, Farkas, J. B. Foresman, J. V Ortiz, J. Cioslowski, and D.J. Fox, Gaussian 16 (Revision C.01), Gaussian, Inc., Wallingford, CT, (2016).

[54] S.F. Boys, and F. Bernardi, “The calculation of small molecular interactions by the differences of separate total energies. Some procedures with reduced errors,” Mol. Phys. **19**(4), 553–566 (1970).

[55] E.R. Johnson, S. Keinan, P. Mori-Sánchez, J. Contreras-García, A.J. Cohen, and W. Yang, “Revealing noncovalent interactions,” J. Am. Chem. Soc. **132**(18), 6498–6506 (2010).

[56] R.F.W. Bader, “Atoms in Molecules,” Acc. Chem. Res. **18**(1), 9–15 (1985).

[57] B. Jeziorski, R. Moszynski, and K. Szalewicz, “Perturbation Theory Approach to Intermolecular Potential Energy Surfaces of van der Waals Complexes,” Chem. Rev. **94**(7), 1887–1930 (1994).

[58] J. Contreras-García, E.R. Johnson, S. Keinan, R. Chaudret, J.P. Piquemal, D.N. Beratan, and W. Yang, “NCIPLOT: A program for plotting noncovalent interaction regions,” J. Chem. Theory Comput. **7**(3), 625–632 (2011).

[59] T.A. Keith, “AIMALL, Version 17.11.14, TK Gristmill Software: Overland Park, KS, USA, (2016).

[60] R.M. Parrish, L.A. Burns, D.G.A. Smith, A.C. Simmonett, A.E. DePrince, E.G. Hohenstein, U. Bozkaya, A.Y. Sokolov, R. Di Remigio, R.M. Richard, J.F. Gonthier, A.M. James, H.R. McAlexander, A. Kumar, M. Saitow, X. Wang, B.P. Pritchard, P. Verma, H.F. Schaefer, K. Patkowski, R.A. King, E.F. Valeev, F.A. Evangelista, J.M. Turney, T.D. Crawford, and C.D. Sherrill, “Psi4 1.1: An Open-Source Electronic Structure Program Emphasizing Automation, Advanced Libraries, and Interoperability,” J. Chem. Theory Comput. **13**(7), 3185–3197 (2017).

[61] H.M. Pickett, “The fitting and prediction of vibration-rotation spectra with spin interactions,” J. Mol. Spectrosc. **148**(2), 371–377 (1991).